Integration of Sentinel-2 Spectral Information with High Spatial Resolution Planetscope Imagery for Wildfire Damage Assessment

Minho Kim (1), Yongil Kim (1)

[1]Seoul National Univ., 1 Gwanak-ro, Gwanak-gu, Seoul 08826, Korea
Email: mhk93@snu.ac.kr; yik@snu.ac.kr

KEY WORDS: Burn area, wildfire, Planetscope, Sentinel-2, histogram matching

ABSTRACT: In the short-term aftermath of a wildfire, quick damage assessment is significant to implement efficient disaster response, but the acquisition of reliable reference data can be difficult. Remote sensing (RS) methods using satellite imagery can provide a rapid means to quantify the distribution (burn area) and level of damage (burn severity) for wildfire damage assessment. However, optical satellite images are limited by their spatial and temporal resolutions. In this study, Planetscope (PS) and Sentinel-2 (S2) images were processed to evaluate the Okgye, Sokho, and Inje wildfires in terms of their burned area using differential images of spectral indices. First, Normalized Burn Ratio (NBR) of S2 images and Normalized Vegetation Index (NDVI) of PS images were processed. The correlation between S2 dNBR and PS dNDVI was found to be 0.9390, suggesting the similarity between the two spectral index calculations. Second, to fully utilize the superior spatio-temporal resolution of PS and the broader spectral range of S2, dNBR spectral information from S2 (20 m spatial resolution) was transferred to the high spatial resolution PS dNDVI result (3 m spatial resolution) by histogram matching. The results revealed that this integrated approach classified the burned area of the Okgye wildfire more accurately because the histogram-matched image was able to discriminate smaller features more clearly, such as patches of bare soil and narrow roads. However, this method struggled to estimate burned area for the Sokcho and Inje wildfire study areas due to overestimation in mixed land cover areas and underestimation in mountainous topography, respectively. Although the performance of the histogram matching method can be scene-specific, the intervals from the histogram-matched results can be used as potential benchmarking values for future wildfire damage assessment using VIS-NIR imagery.

1. INTRODUCTION

Following the outbreak of a wildfire, rapid response is imperative to implement efficient disaster management measures. Under such dire circumstances however, high quality reference data can be difficult to obtain or are inaccessible, while traditional field surveying methods are generally too slow or costly to be used effectively. Alternatively, remotely-sensed satellite imagery can provide vital information of the wildfire at higher temporal frequency, lower costs, wider spatial coverage, and faster processing speeds.

In general, considerable spatio-temporal resolution and wide coverage are required to evaluate the wildfire damage effectively. Recent studies revealed that medium-resolution optical satellite imagery such as Landsat-8 (L8) Operational Land Imager/Thermal Infrared Sensor and Sentinel-2 (S2) MultiSpectral Instrument (MSI) were used most frequently for wildfire burn mapping and evaluation (Navarro et al., 2017; Fernández-García et al., 2018; Sobrino et al., 2019). For wildfire burn estimation, spectral indices are frequently used due to their computational lightness, resistance to terrain relief and shadows, and relatively accurate performance (Fernández-Manso et al., 2016; Fernández-García et al., 2018; Sobrino et al., 2019). Traditionally, the Normalized Difference Vegetation Index (NDVI) has been a popular choice to evaluate wildfire damage because the index can accentuate the spectral characteristics of vegetation in comparison to non-vegetation (including burned areas) at NIR and red wavelengths. For satellite sensors that can sense in the Short-Wavelength Infrared (SWIR) band, such as L8 and S2, the Normalized Burn Ratio (NBR) (Key and Benson, 2003) has become one of the most commonly-used and adopted indices for the detection of wildfire burn scars (Fox et al., 2008) and mapping of burn severity (Cocke et al., 2005; Escuin et al., 2008). The two spectral indices are given by the following band combinations:

$$\mathrm{NDVI} = \frac{\mathrm{NIR}-\mathrm{RED}}{\mathrm{NIR}+\mathrm{RED}} \quad (1)$$

$$\mathrm{NBR} = \frac{\mathrm{NIR}-\mathrm{SWIR}}{\mathrm{NIR}+\mathrm{SWIR}} \quad (2)$$

In comparison to the NIR and red band difference used in NDVI, NBR utilizes the contrast in SWIR and NIR responses reflected between burned areas and healthy vegetation. At times, this difference can provide more meaningful information since the scorched ashes reflect stronger signals in the SWIR range (Miller and Thode, 2007). The characteristics of spectral indices are explained in more detail in Section 3.2 and 3.3. In order to classify

wildfire burn severity, the differential NBR classification scheme revealed by United States Geological Survey (USGS) provides reputable reference values (Key and Benson, 2003) and have been widely used for studies on wildfire burn area and severity mapping (Cocke *et al*., 2005; Miller and Thode, 2007; Sobrino *et al*., 2019). Further explanation is provided in Section 3.3.

Despite their advantages over traditional ground-based methods however, optical satellites can suffer from a trade-off between their spatial and temporal resolutions when applied for wildfire damage assessment. To address this limitation, satellite images with higher spatiotemporal resolution can be used. Planet Labs offers one potential solution by operating a constellation of more than 120 Cubesat units referred to as Planetscope (PS). The Cubesats are lightweight and inexpensive, consisting of essentially a multispectral sensor and downlinking system (Cooley et al., 2017). These nanosatellites provide daily global coverage of the Earth using one Near-Infrared (NIR) and three visible (VIS) bands at about 3 m spatial resolution. PS thus provides a cost-effective solution by acquiring images at shorter revisit times, higher spatial resolution, reasonable pricing, and sufficient coverage of the wildfire target scene (Houborg and McCabe, 2016; Houborg and McCabe, 2018a; Houborg and McCabe, 2018b).

PS possesses superior spatio-temporal resolution over conventional satellites, but can be disadvantageous for wildfire damage assessment due to its lack of an SWIR band and limited spectral bandwidth. Also, using only satellite images can be problematic since factors such as cloud coverage, haze, shadow, insufficient coverage, and inadequate revisit time can limit image acquisition for wildfire damage assessment. Another issue to note is the the application of the USGS burn severity scheme in Korea. This procedure requires additional testing since there is confusion when mapping areas between non-burned and low-severity intervals. Hence, despite the diversity of spectral indices available, there is yet no consensus on the most optimal and robust index for wildfire damage assessment (Miller and Thode, 2007; Fernández-García et al., 2018).

In light of the drawbacks of using the satellites individually, combining the advantages of both conventional satellites and PS would be ideal. This study therefore presents the prospect of exploiting the high spectral resolution of optical satellites and high spatial-temporal resolution of PS. Histogram matching, or histogram specification, is applied in order to combine the information from the different sensors. the spectral information from the coarse spatial resolution domain is transferred to a higher spatial resolution domain, where the wildfire damage can be analyzed at a finer level of detail. This approach is particularly useful if high quality ground truth data or conventionally-used optical satellite images are not available for wildfire damage assessment. This study is organized in the following order: Section 2 introduces the study area and the datasets used to investigate the wildfires. Section 3 presents supporting concepts covered in this research, such as spectral indices and differential images used for wildfire damage assessment. Section 4 reveals the results of wildfire damage assessment in terms of burn area for each study area. Finally, the conclusion provides a summative review of the study and closing remarks on the potential of PS for wildfire damage assessment.

2. DATASETS AND STUDY AREAS

2.1 Study Areas

The Gangwon wildfires in April 2019 refer to three wildfires which engulfed different regions of the province. First, the Okgye wildfire was discovered south of Okgye-myeon in the Gangwon province, where the flames blazed throughout the mountainous regions, but also managed to reach nearby roads and small patches of land. Second, the Sokcho wildfire spread throughout both rural and mountainous regions. Third, the Inje wildfire burned in the forest and mountainous regions in Nam-myeon. According to the disaster response and recovery report issued by Ministry of the Interior and Safety (MOIS) on April 18th, 2019, the Okgye wildfire scorched 714.8 ha, the Sokcho wildfire burned 700 ha, and the Inje wildfire ravaged 342.2 ha of land (MOIS, 2019). Detailed descriptions of the fires are organized in Table 1 where the time date is given in year/month/date format and the time, in Korean Standard Time. These measurements by MOIS were used as reference burn area values for wildfire damage assessment in this study. Subsequent investigations revealed that the fire was triggered by sparks from electrical wires and the wildfire expanded rapidly due to the arid climate, high leaf area, distribution of low-moisture coniferous trees, and high wind velocity (MOIS, 2019). The study areas of the three wildfires are shown in Figure 1 using post-fire PS images.

Table 1. Details on the April 2019 Gangwon-do wildfires

Site	Okgye	Sokcho	Inje
Location	Gangneung-si, Okgye-myeon, Namyang-ri 958	Goseong-gun Toseong-myeon Wonam-ri	Inje-gun Nam-myeon Namjeon-ri 503-2
Discovered	19/4/4 (23:46)	19/4/4 (19:17)	19/4/4 (14:45)
Extinguished	19/4/5 (16:54)	19/4/5 (08:15)	19/4/6 (12:00)
Burn Area	714.8 ha	700 ha	342.2 ha

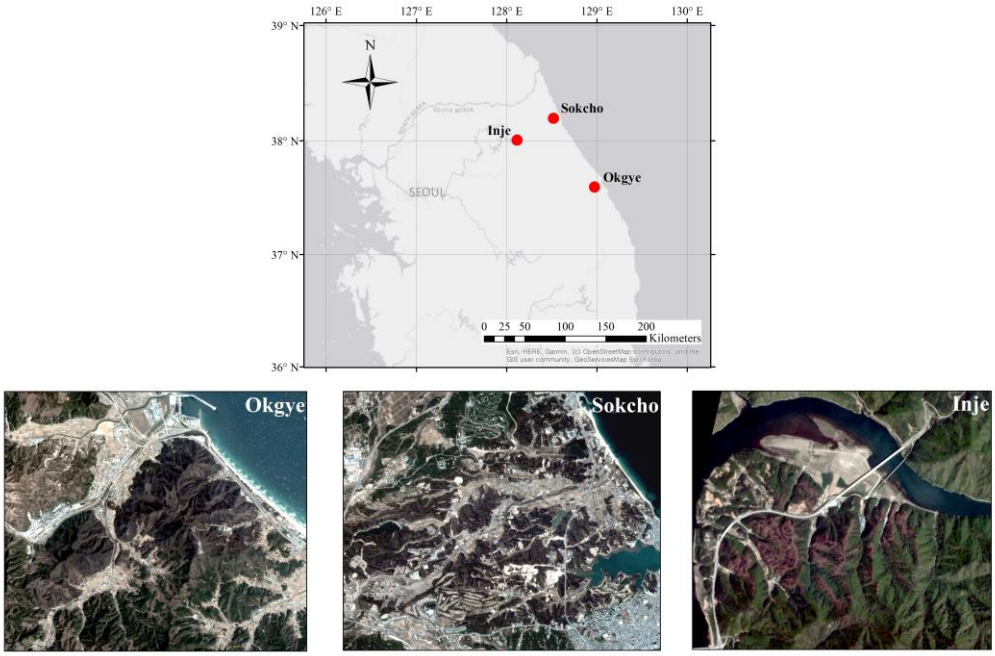

Figure 1. Map of study areas with each wildfire site displayed using PS post-fire images.

2.2 Datasets

Upon considering an appropriate dataset of satellite imagery for spectral image integration, S2 imagery was selected based on the sensor's well-calibrated spectral bands (including SWIR bands), narrow bandwidths, accessibility of free data, relatively high spatial resolution, and reasonable revisit time (when both S2A and S2B units are used together). S2 images are provided as Level-1C images while PS images are provided in three product types: Level-1B Basic scene, Level-3A Visual/Analytic ortho-scene, and Level-3B Visual/Analytic ortho-tile. Level-3 products are geometrically and radiometrically corrected images that are ready for further analysis. Basic specifications of the two satellites are shown in Table 2, and the spectral response functions of the two sensors are plotted together in Figure 2.

Table 2. Specifications of PS and S2 satellite imagery

Specifications	PS	S2
Operator	Planet Labs	European Space Agency (ESA)
Spatial Resolution	3.7 m (at nadir)	10 m (VIS-NIR), 20 m (red-edge, SWIR), 60 m (cirrus, water vapor)
Spectral Bands	4 bands	13 bands
Temporal Resolution	Daily	5 days (S2A and S2B combined)

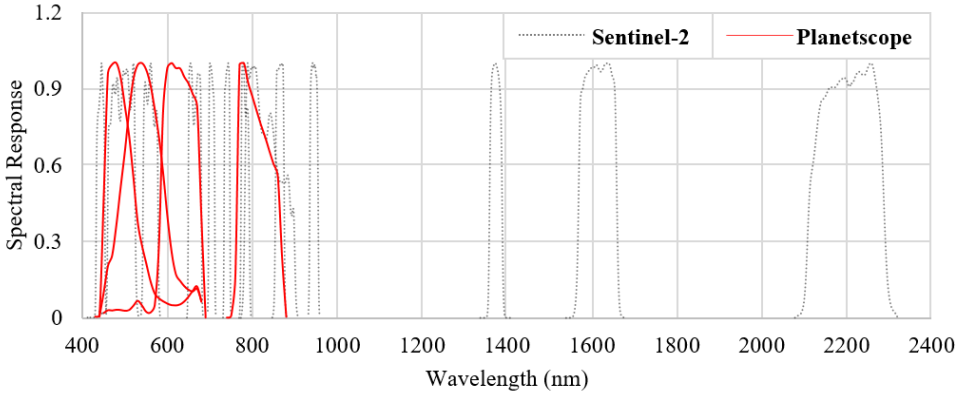

Figure 2. Comparison of S2 and PS spectral response functions.

In general, previous studies claimed that PS images suffer from poor radiometric resolution, low signal-to-noise ratio, and cross-sensor inconsistencies (Cooley et al., 2017; Houborg and McCabe, 2018a; Houborg and McCabe, 2018b). In response to these issues, Planet Labs processes PS image acquisitions using various types of corrections and calibration/validation procedures. In-house correction methods include pre-launch and on-orbit sensor calibration, rigorous orthorectification using fine DEM and bundle adjustment algorithm, and mosaicking of acquired image stitches (Cooley et al., 2017; Houborg and McCabe, 2016; Houborg and McCabe, 2018b). Since this research is focused on post-processing the acquired PS images for wildfire damage assessment, Level-3 Analytic PS ortho-scene images were selected to minimize preprocessing steps in this study. Also, S2 Level-1C images were used and corrected to Level-2A images. PS and S2 images were obtained based on minimal cloud coverage, sun zenith angle, revisit time, and overall scene quality. The detailed specifications of the datasets used in this study are listed in Table 3. To note, multiple PS images were required when the coverage of a single image was too small to cover the entire wildfire.

Table 3. Specifications of input datasets used for wildfire damage assessment

Site	Sensor	Acquisition Date	Difference in Dates	Number of Scenes for Full Coverage	Sensor Type	Cloud (%)
Okgye	PS	04/03	5 days	2	Flock-3P-68 (Dove 1004)	0
		04/08		2	Flock-3P-77 (Dove 0F28)	
	S2	04/03		1	S2A	3
		04/08		1	S2B	2.5
Sokcho	PS	03/14	31 days	4	Flock-2k 37 (Dove 1050)	0
					Flock-3p 34 (Dove 103B)	
		04/15		2	Flock-3m 2 (Dove 0F02)	0
	S2	03/14		1	S2A	0
		04/15		1	S2B	0
Inje	PS	04/03	30 days	2	Flock-2p 12 (Dove 0E3A)	0
		05/03		2	Flock-2p 9 (Dove 0E26)	
	S2	04/03		1	S2A	5.6
		05/03		1	S2B	0

3. METHODOLOGY

3.1 Preprocessing Steps

The S2 images were processed using a common architecture for Sentinel toolboxes called Sentinels Application Program (SNAP) version 6.0. The first step for preprocessing was to correct the input images to Level-2 products using Sen2Cor by ESA. This module performs atmospheric, terrain, and cirrus correction of Top of Atmosphere (TOA) from a Level-1C input image to generate Level-2A surface reflectance products (Louis et al., 2016). Second, band resampling was processed to match the different spatial resolutions of S2's spectral bands as shown in Table 2. Third, unnecessary water bodies and noise values were masked from the image. This filtering step was processed by using the Normalized Difference Water Index (NDWI) (McFeeters, 1996) where, in general, values greater than zero indicate the presence of water or moisture.

$$\mathrm{NDWI} = \frac{\mathrm{GREEN}-\mathrm{NIR}}{\mathrm{GREEN}+\mathrm{NIR}} \tag{3}$$

Lastly, the images were re-projected to the Universal Transverse Mercator 52N coordinate system (focused on the Korean peninsula) and fitted according to a subset of the studied wildfire region. For this study, the PS images were processed using the image analysis software, Environment for Visualizing Images (ENVI) version 5.3. In spite of Planet Lab's rigorous corrections and calibration/validation procedures, additional preprocessing steps were still required. Initially, multiple ortho-scene products are required for full coverage of the wildfire. Since the images were acquired from different PS sensors, seamless image mosaicking of the images is needed. Noisy data and water bodies should then be filtered prior to analysis using NDWI thresholding. Lastly, the images are re-projected and fitted to the subset area. The ensuing masking and subset steps were conducted in a similar manner to that of S2.

3.2 Spectral Indices for Wildfire Damage Assessment

The spectral indices, NDVI and NBR are particularly sensitive to the spectral responses reflected by vegetation and burned areas by manipulating the spectral responses acquired by the red, NIR, and SWIR bands. With regards to the former index, NDVI exploits the difference in spectral response recorded between healthy vegetation, which reflect strongly in the red-NIR range, and burned areas from wildfires, which reflect lower responses (Lentile et al., 2006). As for the latter spectral ratio, NBR manipulates bandwidths that are characteristic of water absorption such as S2 MSI's SWIR bands 11 and 12 to capture a larger range of post-fire variation (Tran et al., 2018).

3.3 Differential Image Generation

Post-fire images with minimal cloud coverage, favorable weather conditions, and full scene coverage may not be available in the first place. In this case, mono-temporal analysis using a single image can cause confusion when interpreting features which exhibit similar spectral characteristics, such as shadows and burned areas (Viana-Soto et al., 2017). The present study focused on the bi-temporal analysis of spectral ratio images, similar to change detection, but used only the differential images to minimize the effect of shadows and to manipulate the spectral characteristics between burned areas and healthy vegetation. The analysis of differential images of pre- and post-fire images enabled more accurate assessment of the wildfire burn area and severity because the differential result can take into account unchanged features and low vegetation cover in the pre-fire scene (Fox et al., 2008). To create a differential image, the difference in NBR (dNBR) and difference in NDVI (dNDVI) between pre- and post-fire images are calculated.

$$\mathrm{dNBR} = \mathrm{NBR}_{\mathrm{pre}} - \mathrm{NBR}_{\mathrm{post}} \tag{4}$$

$$\mathrm{dNDVI} = \mathrm{NDVI}_{\mathrm{pre}} - \mathrm{NDVI}_{\mathrm{post}} \tag{5}$$

Table 4. USGS classification scheme on wildfire burn severity using dNBR

dNBR Interval	Burn Severity
< -0.25	High post-fire regrowth
-0.25 to -0.1	Low post-fire regrowth
-0.1 to +0.1	Non-burn
0.1 to 0.27	Low-severity burn
0.27 to 0.44	Moderate-low (Mod-low) severity burn
0.44 to 0.66	Moderate-high (Mod-high) severity burn
> 0.66	High-severity burn

In particular, previous studies demonstrated the similarity between dNBR and dNDVI for detecting burned areas, given the nature of the two spectral indices (Fox et al., 2008; Navarro et al., 2017). The two indices have demonstrated significant overlap in values with each other, since burned vegetation and bare soil return similar spectral signals of low absorption in the NIR range and high reflectance in the SWIR and Red range. (Fox et al., 2008). Bare surfaces and areas of minimal to no change yield values close to zero, while highly changed, or in this context, highly burned surfaces display large positive values. However, the intervals in Table 4 can vary according to multiple factors, including pre-fire vegetation density, forest type, land cover type, and climate (Miller and Thode, 2007; Fox et al., 2008; Tran et al., 2018).

3.4 Histogram Matching

Histogram matching, or histogram specification, is defined as matching the pixel value distribution from a reference image, denoted as P_R, to an input image, referred to as P_A, by using a mapping function which describes the transfer of pixel values (Gonzalez and Woods, 2002). In principle, histogram matching is based on computing the cumulative distributions for each image and mapping the input image's value at a given threshold point to the reference value that has the same probability (Gonzalez and Woods, 2002). This procedure is displayed in Figure 3. When converting to the histogram-matched (HM) image, the value of $P_A(x_i)$ is found where the reference and input images are related such that:

$$P_{A'}(x_i) \approx P_R(x_i) \tag{5}$$

Based on this threshold value, x_i is allocated to its new position x_i' on the input image histogram. The matching

procedure can be expressed by a combination of the two distribution functions as:

$$x_i' = P_R^{-1} P_A(x_i) \tag{6}$$

The result is HM image $P_{A'}$ which contains information from the reference image's domain mapped to that of the input image. In this study, histogram matching is performed to transfer the S2 spectral information to the high spatial resolution PS image, provided that the images reflected similar characteristics in their scenes.

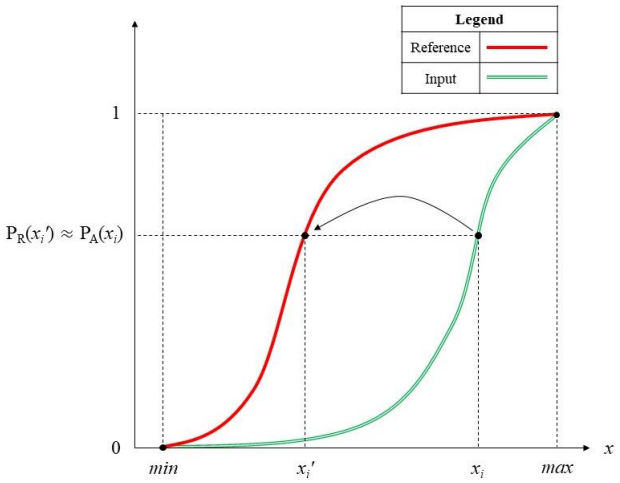

Figure 3. Graphical visualization of histogram matching.

3.5 General Workflow

The following workflow shown in Figure 4 displays the specific processing steps executed in this study.

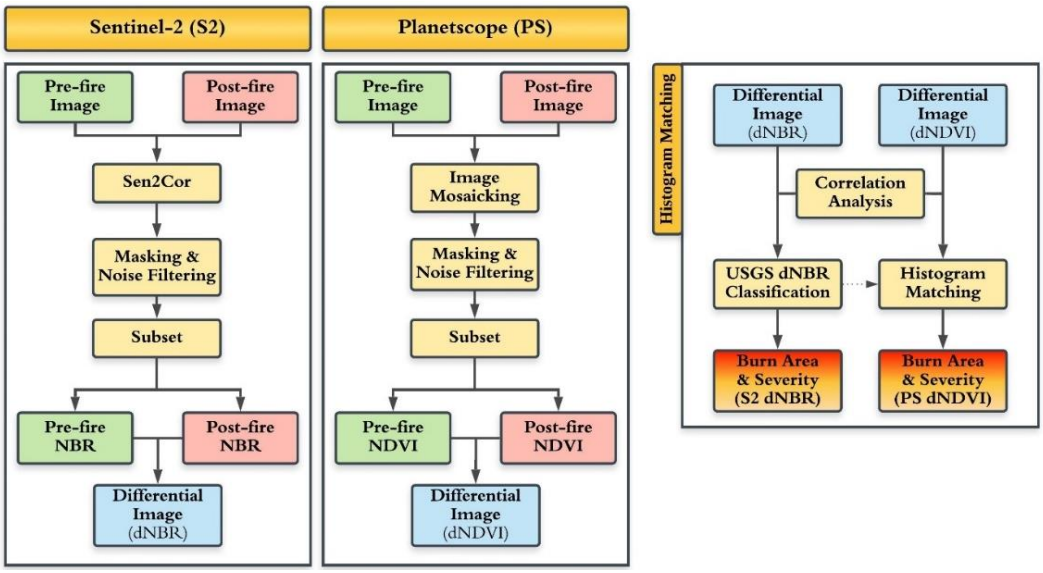

Figure 4. General workflow of present study showing pre-processing (left) and damage assessment (right).

4. RESULTS AND DISCUSSION

4.1 Correlation of Spectral Indices

Prior to histogram matching, regression analysis of the two differential images, S2 dNBR and PS dNDVI, were compared to evaluate the degree of similarity found in the computed images. Based on the subset scenes, the Okgye image returned the highest correlation coefficient of 0.939, as shown in Figure 5 (a). The other two images also displayed relatively high correlation. The Okgye scene revealed particularly high correlation since the two compared

differential images had clear bimodal distributions. In other words, the burned and non-burned areas were well-separated. In contrast, the Sokcho scene consisted of mixed land covers, as reflected by the wider range in high density points distributed near zero. The Inje scene was filled with forests and mountains and, as a result, the majority of the points were found to be than zero.

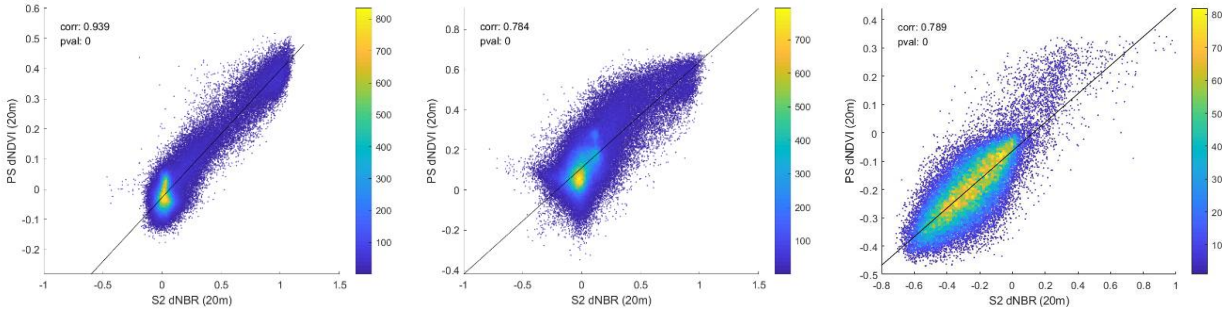

(a) (b) (c)

Figure 5. Regression analysis of S2 dNBR and PS dNDVI. (a) Okgye (Correlation coefficient of 0.939). (b) Sokcho (Correlation coefficient of 0.784). (c) Inje (Correlation coefficient of 0.789).

4.2 Wildfire Burn Area Estimation and HM Results

The computed differential image of S2 dNBR and PS dNDVI are provided in Table 5 where wildfire burn scars are depicted using a lighter white tone, since higher values indicate greater change for each spectral index. The left and right portions of the Inje PS dNDVI and Okgye S2 dNBR, respectively, were not included in the subset because of the lack of coverage at the time of acquisition. As mentioned in Fox et al. (2008), the dNBR and dNDVI images exhibit similar high values in burned areas. While the two differential images showed similar burn area extents, the difference in spatial resolution is reflected by the finer details in the PS dNDVI image.

Table 5. Comparison of differential images of spectral index calculations

	Okgye	Sokcho	Inje
(a) PS dNDVI	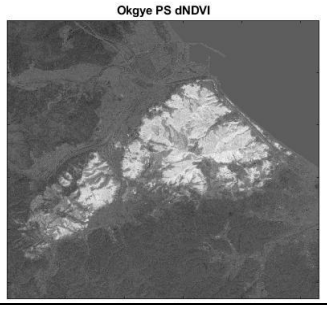	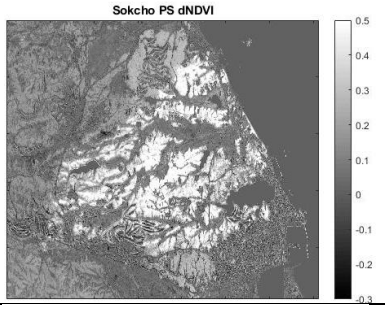	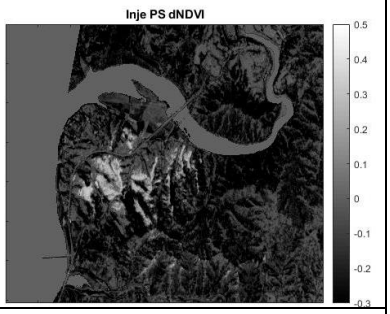
(b) S2 dNBR	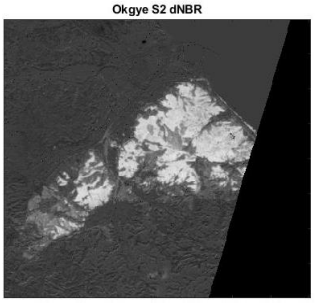	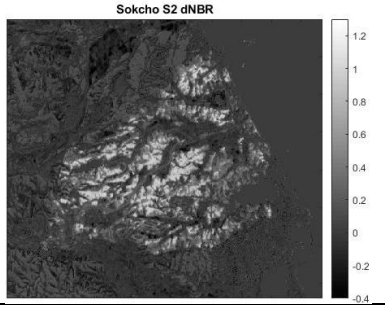	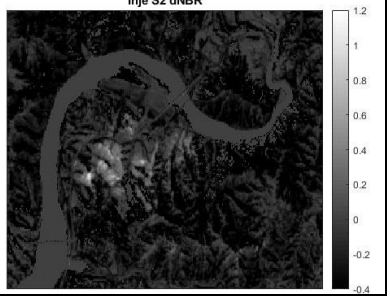

The S2 dNBR images were used as reference images to histogram match the input PS dNDVI images. As shown in Table 6, the reference images used dNBR burn severity values in Table 4 to histogram match points onto the PS dNDVI image for each wildfire site. On the PS dNDVI image, the HM threshold values less than zero ("regrowth" intervals) were omitted from because, in essence, these areas signified non-burn pixels. Non-burn regions were labelled without any color in the images and the subsequent threshold values were adjusted according to the histogram matching procedure. The resulting HM images are displayed in Figure 6.

Table 6. PS dNDVI intervals derived from S2 dNBR by histogram matching

dNBR	Interval	HM PS dNDVI			Burn Severity
		Okgye	Sokcho	Inje	
Min		-	-	-	Non-burn
-0.1		0	0	0	
0.1		0.178	0.303	0.229	Low-severity burn
0.27		0.232	0.372	0.254	Moderate-low (Mod-low) severity burn
0.44		0.286	0.441	0.279	Moderate-high (Mod-high) severity burn
0.66		0.356	0.531	0.312	High-severity burn
Max		0.504	0.713	0.361	Extreme or anomaly values

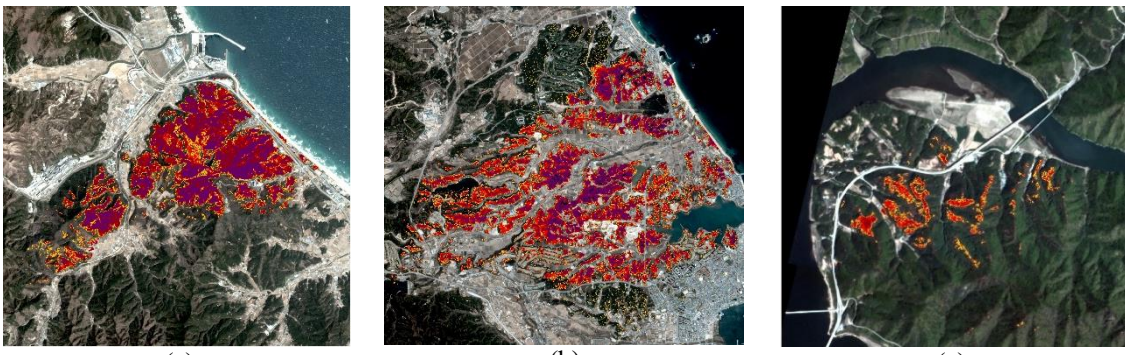

(a) (b) (c)

Figure 6. HM PS dNDVI images showing wildfire burn scar. (a) Okgye. (b) Sokcho. (c) Inje.

4.3 Wildfire Damage Assessment

Wildfire damage was evaluated using the HM PS dNDVI images provided in Figure 6. The resulting burned areas were calculated by summing HM intervals classified as burned area from "Low" to Extreme" burn severity intervals shown in Table 7. From these results, S2 dNBR estimates tended to overestimate the burned area for Okge and Sokcho test sites when using Table 4 for burn severity classification. After visual inspection and removing the "Low" severity interval, the burned area estimates returned much closer estimates to the reference values. This overestimation can be attributed to the difficulty of differentiating areas of low burn severity with non-burn areas.

Among the HM results, the HM PS dNDVI image for the Okgye wildfire produced the most accurate result. The HM image for Sokcho yielded an estimate in between the two S2 dNBR estimates, suggesting a slight overestimation in burned area classification. To elaborate, for the Okgye site, the burned areas were clustered together compared to the non-burned regions, whereas for the Sokcho site, the burn scar was distributed more sparsely within a mixed, heterogeneous area. In contrast, all images of the Inje wildfire underestimated burned area, likely due to confusion caused by the mountainous topography and relatively low levels of differential spectral index values.

While dNBR results can be classified for burn severity using Table 4, as mentioned, there is yet no agreement on the most optimal interval for burn severity classification when using VIS-NIR bands. However, since histogram matching can be subjective and scene-specific, additional tests using the HM intervals are required in order to consolidate the threshold values for effective classification. The results from Table 6 can thus be used as a preliminary benchmark for future burn severity thresholding when using PS images for burn severity grading.

Table 7. Evaluation of burned area estimates from S2 dNBR and HM PS dNDVI

Total Burn	Okgye Burned Area (ha)	Sokcho Burned Area (ha)	Inje Burned Area (ha)
Reference (MOIS, 2019)	714.8	700	342.2
S2 dNBR (Low to High)	1472.40	1079.72	15.02
S2 dNBR (Mod-Low to High)	913.92	803.28	5.13
HM PS dNDVI	709.86	909.43	14.34

5. CONCLUSION

In this study, damage assessment of the three Gangwon wildfires in Okgye, Sokcho, and Inje was evaluated in terms of burned area. From an ecological standpoint, even small burned patches are of utmost importance since the patch size and burn severity can ultimately affect the number of victims from the fire. In light of this consideration, this study demonstrated that PS images can be used with, and potentially instead of, other conventionally-used satellite imagery, given the shorter revisit time and superior spatial resolution of PS, to perform more accurate and rapid disaster response to wildfire damage. From this study, S2 imagery was used as a reference source to transfer their high spectral information to PS images and compensate for the spectral limitation of PS sensors. Spectral information from S2 dNBR was transferred to a higher spatial resolution domain in PS dNDVI, provided that the two spectral indices yielded a reasonable level of correlation in the compared scenes. The threshold values from S2 dNBR were integrated via histogram matching to produce HM intervals in the PS dNDVI image. The HM PS dNDVI result for Okgye generated the most accurate estimate of burned area of 709.86 ha. On closer inspection, the HM image was able to discriminate smaller patches of land and narrow roads compared to the S2 dNBR image. For Sokcho and Inje on the other hand, the HM PS dNDVI images overestimated and underestimated the burn area to a considerable extent. These results suggest that sparsely distributed burn area, especially in regions of mixed land cover, as well as mountainous terrain and shadows can influence burn area estimations significantly. With regards to burn severity classification, since there is yet no global and robust spectral index for burn area and severity mapping, nor a reference classification scheme for dNDVI, the results of this study can be used as a preliminary benchmark for future wildfire damage assessment. Additional steps are required to test the burn severity thresholds for different acquisition times in order to develop a more concrete reference standard for effective wildfire burn area mapping.

ACKNOWLEDGEMENT

This research was supported by a grant (2019-MOIS32-015) of Disaster-Safety Industry Promotion Program funded by Ministry of Interior and Safety (MOIS, Korea). Image courtesy of Planet Labs, Inc. Planetscope imagery is provided through the Planet's Education and Research program.

REFERENCES

Cocke, A. E., P. Z. Fulé, and J. E. Crouse, 2005. Comparison of burn severity assessments using Differenced Normalized Burn Ratio and ground data, International Journal of Wildland Fire, 14 (2), 189-198.

Cooley, S., L. Smith, L. Stepan, and J. Mascaro, 2017. Tracking dynamic northern surface water changes with high-frequency Planet CubeSat imagery, Remote Sensing, 9 (12), pp. 1306.

Escuin, S., R. Navarro, and P. Fernandez, 2008. Fire severity assessment by using NBR (Normalized Burn Ratio) and NDVI (Normalized Difference Vegetation Index) derived from LANDSAT TM/ETM images, International Journal of Remote Sensing, 29 (4), pp. 1053-1073.

Fernández-García, V., M. Santamarta, A. Fernández-Manso, C. Quintano, E. Marcos, and L. Calvo, 2018. Burn severity metrics in fire-prone pine ecosystems along a climatic gradient using Landsat imagery, Remote Sensing of Environment, 206, pp. 205-217.

Fernández-Manso, A., O. Fernández-Manso, and C. Quintano, 2016. SENTINEL-2A red-edge spectral indices suitability for discriminating burn severity, International Journal of Applied Earth Observation and Geoinformation, 50, pp. 170-175.

Fox, D. M., Maselli, F., and Carrega, P., 2008. Using SPOT images and field sampling to map burn severity and vegetation factors affecting post forest fire erosion risk. Catena, 75 (3), pp. 326-335.

Gonzalez, R. C. and R. E. Woods, 2002. Digital Image Processing, Prentice Hall Press, New Jersey, USA.

Houborg, R. and M. McCabe, 2016. High-resolution NDVI from Planet's constellation of earth observing nano-satellites: a new data source for precision agriculture, Remote Sensing, 8 (9), pp. 768.

Houborg, R. and M. McCabe, 2018a. A Cubesat enabled spatio-temporal enhancement method (CESTEM) utilizing Planet, Landsat and MODIS data, Remote Sensing of Environment, 209, p. 211-226.

Houborg, R. and M. McCabe, 2018b. Daily retrieval of NDVI and LAI at 3 m resolution via the fusion of CubeSat, Landsat, and MODIS data. Remote Sensing, 10 (6), pp. 890.

Key, C. H. and N. C. Benson, 2003. The Normalized Burn Ratio (NBR): A Landsat TM radiometric measure of burn severity, U.S. Department of the Interior, U.S. Geological Survey, Northern Rocky Mountain Science Center.

Lentile, L. B., Z. A. Holden, A. M. Smith, M. J. Falkowski, A. T. Hudak, P. Morgan, S. A. Lewis, P. E. Gessler, and N. C. Benson, 2006. Remote sensing techniques to assess active fire characteristics and post-fire effects, International Journal of Wildland Fire, 15 (3), pp. 319-345.

Louis, J., V. Debaecker, B. Pflug, M. Main-Knorn, J. Bieniarz, U. Mueller-Wilm, E. G. Cadau and F. Gascon, 2016. S2 SEN2COR: L2A processor for users. Proc. of the Living Planet Symposium, Prague, Czech Republic, May

9-13, pp. 9-13.
McFeeters, S. K., 1996. The use of the Normalized Difference Water Index (NDWI) in the delineation of open water features, International Journal of Remote Sensing, 17 (7), pp. 1425-1432.
Miller, J. D. and A. E. Thode, 2007. Quantifying burn severity in a heterogeneous landscape with a relative version of the delta Normalized Burn Ratio (dNBR), Remote Sensing of Environment, 109 (1), pp. 66-80.
Ministry of the Interior and Safety, 2019. 20190418 Gangwon East-Sea Irwon wildfire response - recovery report (11AM).https://www.mois.go.kr/frt/bbs/type001/commonSelectBoardArticle.do? bbsId=BBSMSTR000000000336&nttId=70191, Accessed on Jul. 22, 2019 (In Korean).
Navarro, G., I. Caballero, G. Silva, P. C. Parra, Á. Vázquez, and R. Caldeira, 2017. Evaluation of forest fire on Madeira Island using S2A MSI imagery, International Journal of Applied Earth Observation and Geoinformation, 58, pp. 97-106.
Sobrino, J. A., R. Llorens, C. Fernández, J. M. Fernández-Alonso, and J. A. Vega, 2019. Relationship between soil burn severity in forest fires measured in situ and through spectral indices of remote detection, Forests, 10 (5), pp. 457.
Tran, B., Tanase, M., Bennett, L., and Aponte, C., 2018. Evaluation of spectral indices for assessing fire severity in Australian temperate forests. Remote Sensing, 10 (11), pp. 1680.
Viana-Soto, A., I. Aguado, and S. Martínez, 2017. Assessment of post-fire vegetation recovery using fire severity and geographical data in the Mediterranean region (Spain), Environments, 4 (4), pp. 90.